NJC

Accepted Manuscript

This article can be cited before page numbers have been issued, to do this please use: K. H. Markiewicz, P. Mikasz, K. Poltorak, I. Misztalewska, S. Wojtulewski, A. Majcher, E. Fornal and A. Z. Wilczewska, *New J. Chem.*, 2016, DOI: 10.1039/C6NJ01938B.

View Article Online
DOI: 10.1039/C6NJ01938B

Journal Name

ARTICLE

Magnetic nanoparticles with chelating shells prepared by RAFT/MADIX polymerization

Received 00th January 20xx,
Accepted 00th January 20xx

DOI: 10.1039/x0xx00000x

www.rsc.org/

Karolina H. Markiewicz,[a]† Paula Zembko,[a] Katarzyna Półtorak,[a] Iwona Misztalewska,[a] Sławomir Wojtulewski,[a] Anna M. Majcher[b], Emilia Fornal[c] and Agnieszka Z. Wilczewska[a]†

In this paper is presented the preparation of multifunctional materials based on magnetic nanoparticles (MNP) and original thiosemicarbazide derivatives. Synthesized nanohybrids consist of iron oxide core and polymeric shell which possess ability to complex metal ions. They exhibit superparamagnetic properties and can thus be easily separated from complex mixtures by using an external magnetic field (facile separation, purification and recyclability). Synthesized carbamohydrazonothioate derivatives were polymerized on dithiocarbonate-coated MNP using RAFT/MADIX (reversible addition-fragmentation transfer/macromolecular design by interchange of xanthates) method. Three types of nanohybrids were obtained and their physicochemical properties were investigated. The ability of nanohybrids to complex palladium(II) ions and spectroscopic properties of the obtained materials were studied. Additionally, hemolytic activity tests of polymer-coated particles were performed in order to confirm their potential in biomedical applications.

Introduction

Magnetic nanoparticles (MNP) are an emerging class of materials for applications in catalysis, nanomedicine, and environment protection.[1–3] Bare MNP tend to agglomerate and phase separate in solution, thus, it is essential to stabilize them with a protecting shell. Mostly, polymers are favored over small molecules as they can ensure an efficient stabilization of nanoparticles and give the possibility to control chemical composition (homopolymer, copolymer) and properties (*e.g.* hydrophobic, hydrophilic) of a shell.[4] On the other hand, anchoring polymers to MNP ensures fast separation of such nanohybrids, good recovery after using and also enables reapplication of the material. Additionally, a suitably designed polymeric shell can offer some extra functions (*e.g.* biocompatibility, resistance to physiological conditions (pH or enzymes), complexing properties or biological activity) leading to a multifunctional polymer-magnetic nanohybrids.

Herein we describe the preparation of functional (complexing and easily separable) polymer-magnetic nanohybrids using iron oxide nanoparticles and original thiosemicarbazide-based monomers. Thiosemicarbazide and its derivatives are excellent chelating ligands for transition metal ions due to their mixed hard-soft donor character and versatile coordination behavior.[5–13] Furthermore, they exhibit interesting biological properties (*i.e.* antibacterial, antiviral, and antineoplastic activity) related to their ability to diffuse through a semipermeable cell membranes.[13–17] Low costs and facility of their synthesis are additional factors justifying their wide applications in medicinal[18–20] and analytical chemistry[21–24]. As thiosemicarbazide-based ligands are broadly used in various fields, recovery of their metal complexes is of great importance. Anchoring this type of ligands on magnetically separable solid phase is a promising solution.

In this study, RAFT/MADIX (reversible addition-fragmentation transfer/macromolecular design by interchange of xanthates) polymerization was employed to form shells around MNP. RAFT/MADIX technique is a type of controlled radical polymerization which uses xanthates/dithiocarbonates (chain transfer agents) to mediate polymerization process.[25,26] This method enables an excellent control of growth, composition and architecture of polymers.[27] It can be easily performed in mild conditions and is compatible with a huge variety of monomers.[4,27,28]

In 'grafting from' approach initial immobilization of chain transfer agents (CTA) on a nanoparticle surface is followed by polymerization of vinyl monomer. CTA is anchored to a nanoparticle surface by its R-group and consequently act as propagating leaving group (polymer chains are grown directly from a nanoparticle surface).[29] There are only several reports describing covalent modification of MNP with dithiocarbonates, including our previous results.[2,30–33]

Three types of polymer-magnetic nanohybrids were obtained using thiosemicarbazide-based monomers. Their metal complexing abilities were studied. Additionally, hemocompatibility of monomer and polymer-coated MNP was evaluated to confirm the interest of using such nanohybrids in biomedical fields. It is worth nothing that there are only a few reports describing polymers containing

[a] *Institute of Chemistry, University of Bialystok, Ciolkowskiego 1K, 15-245 Bialystok, Poland.*
[b] *Jagiellonian University, Faculty of Physics, Astronomy and Applied Computer Science, prof. S. Lojasiewicza 11, 30-348 Cracow, Poland.*
[c] *EMF Lab Emilia Fornal, Paderewskiego 14/44, 20-860 Lublin, Poland.*
† Dr Agnieszka Z. Wilczewska, agawilcz@uwb.edu.pl
† Mrs Karolina H. Markiewicz, k.markiewicz@uwb.edu.pl
Electronic Supplementary Information (ESI) available: [NMR (^{1}H, ^{13}C, 2D), FT IR, LC MS/MS, TG/DTG, UV-Vis, and fluorescence data]. See DOI: 10.1039/x0xx00000x

View Article Online
DOI: 10.1039/C6NJ01938B

thiosemicarbazide moiety,[16,34,35] and none of them concerns polymerization at the surface of magnetic nanoparticles.

Results and discussion

Synthesis of bifunctional monomers. The synthesis of ligand involved two reactions. Initially, terminal amine group of thiosemicarbazide (TSC) was protected in the reaction with benzaldehyde (Figure S1-S2). Next, purified benzaldehyde thiosemicarbazone (BTSC) was treated with 4-chloromethyl styrene (CMS). The whole process is presented in Figure 1. Operating conditions in the second reaction were optimized to obtain the highest yield of the product. In order to avoid undesirable polymerization reaction of vinyl functions the reaction was performed in room temperature without the access of light and in the presence of polymerization inhibitor.

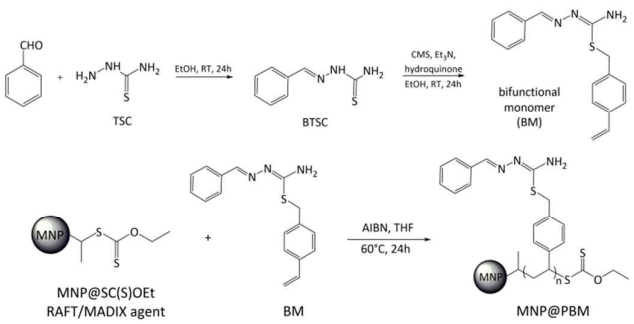

Figure 1. Synthesis of bifunctional thiosemicarbazone-based monomer and its RAFT/MADIX polymerization on dithiocarbonate-coated MNP.

The obtained product was purified and characterized by NMR (^{1}H, ^{13}C, 2D), FT IR, LC MS/MS spectroscopies (Figure S3-S7) and elemental analysis (CHNS). An X-ray diffraction analysis was also taken to determine the molecular structure of the product (Figure 2).

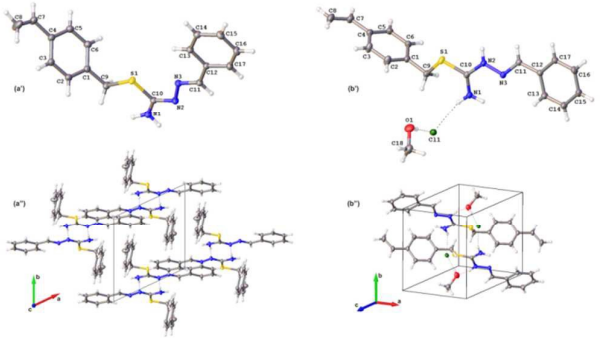

Figure 2. Molecular structures (a'), (b') and crystal structures (a'') (b'') of BM and BMS respectively (hydrogen bonds - dashed lines). The figure was prepared with OLEX2[36].

In order to prepare monomer which could be polymerized in less toxic polar solvents the obtained bifunctional monomer was transformed into its hydrochloric salt (BMS) (Figure S9-S13). The changes in NMR and FT IR spectra of BMS in respect to BM indicate differences in the structure of both products. Additionally, determined by XRD molecular structure of BMS is different (Figure 2). A summary of relevant crystallographic data for both BM and BMS is given in the Table S1. CCDC-1049864 (BM) and CCDC-1049967 (BMS) contains the supplementary crystallographic data for this paper. These data can be obtained free of charge from the Cambridge Crystallographic Data Centre via www.ccdc.cam.ac.uk/data_request/cif.

Surface initiated RAFT/MADIX polymerization. RAFT/MADIX polymerization technique was employed to conduct polymerization of the obtained monomers on the surface of dithiocarbonate-coated magnetic nanoparticles (Figure 1). In this study, iron oxide core-aminosilane shell nanoparticles were used. Their synthesis, characterization and applications have been previously described.[37] Ethyl dithiocarbonate (xanthate) - RAFT/MADIX chain transfer agent - was covalently bonded to the surface of nanoparticles according to the reported method.[32] Polymerization was realized by simple introduction of a dithiocarbonate-coated magnetic nanoparticles (MNP@SC(S)OEt) to a conventional free-radical system (monomer and initiator). Prior reaction RAFT/MADIX agent, monomer, initiator and solvent were sonicated until a homogeneous suspension was formed. The reactions were carried at the constant temperature for 24h under argon gas protection. Due to the differences in the solubility of monomers (BM and BMS) polymerization reactions were performed in different solvents. Initially, several solvents were investigated e.g. toluene, THF, methanol, and ethanol. The best results *i.e.* the highest thicknesses of polymeric shells (determined by TG analysis) were obtained using THF (BM) and ethanol (BMS) as the solvents. AIBN was used as initiator and it was added in 4 portions, at the beginning of the polymerization, after 2 hours, 4 hours and 16 hours of stirring. After reactions, the cycle of redispersion in solvent and magnetic separation was used several times to rinse unreacted monomer, free polymer chains and obtain 'pure' polymer-grafted nanoparticles. In each case mass increase after polymerization was observed. As a result, two types of nanohybrids were obtained: MNP@PBM and MNP@PBMS.

Free radical polymerizations and RAFT/MADIX polymerizations (using O-ethyl-S-(1-methoxycarbonyl)ethyldithiocarbonate as CTA[26]) of both monomers were also carried out in solution. In all cases, in the course of reactions, formation of poorly soluble solid fractions was observed. Apparently, growing chains were excluded during reaction due to decrease of solubility. ^{1}H NMR spectra of these fractions confirmed polymerization. The signals of vinyl protons (at 5.2, 5.7 and 6.7 ppm) disappeared, the peaks of aromatic protons (7.3, 7.8 ppm) become broader, and also new broad signals related to CH and CH_2 protons in polymer chains appeared in the range 1-1.7 ppm. Additionally, in the cases of RAFT/MADIX polymerization, the absence of CTA agent signals in the NMR spectra of soluble residuals confirmed participation of CTA in polymerization process. It is worth of pointing out that during polymerization performed on MNP@SC(S)OEt particles size exclusion, which is inevitable during polymerization carried out in solution, does not take place. In this regard, polymerization on MNP@SC(S)OEt surface is not limited by the solubility of growing polymer chains.

The modifications of the MNP@SC(S)OEt surface were investigated by ATR FT IR spectroscopy. The spectra of the obtained monomers and polymer-grafted nanoparticles are presented in the Figure 3.

View Article Online
DOI: 10.1039/C6NJ01938B

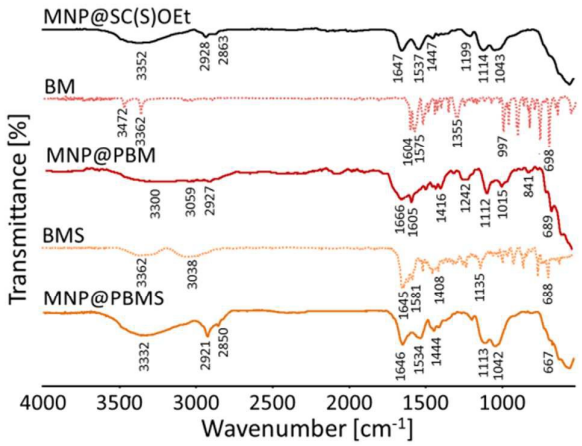

Figure 3. ATR FT IR spectra of obtained monomers and polymer-magnetic nanohybrids.

In each spectrum of nanoparticles a similar set of bands can be observed. The existence of magnetic core is indicated by broad band at 550-570 cm^{-1} which corresponds to the Fe-O stretching modes. The band at around 1000-1150 cm^{-1} can be ascribed to the Si-O, Si-O-Si and Fe-O-Si bonds vibrations (these bonds created by sol gel method with (3-aminopropyl)trimethoxysilane are present in the starting material - MNP@SC(S)OEt).[32] The bands at around 2900 cm^{-1} corresponding to C–H stretching modes and broad band with the maximum around 3300 cm^{-1} related to N-H vibrations are also present in each spectrum. In the spectrum of MNP@SC(S)OEt nanoparticles, the absorption modes at 1647 cm^{-1} and 1537 cm^{-1} correspond to the vibrations of amide moieties (C=O stretching, N-H bending and C-N stretching). The peaks at 1199 cm^{-1} and at 1043 cm^{-1} can be assigned to the C-O-C and S-C-S stretching vibrations of ethyl xanthate groups. After polymerization reactions changes in the spectra of MNP@PBM and MNP@PBMS samples are observed, primarily, in the fingerprint region. For example, at 660-690 cm^{-1} C-H bending vibrations of aromatic rings can be seen. Furthermore, additional (in comparison to MNP@SC(S)OEt) bands around 1200-1450 cm^{-1} appeared which can be ascribed to vibrations of CH and CH_2 groups in polymer chains. The stretching modes of C=N, and $C=C_{Ar}$ groups showed up at 1500-1670 cm^{-1} changing intensity and shape of bands in this region.

Thermogravimetric studies were performed in order to investigate thermal properties of the obtained nanoparticles. Figure 4 shows TG (4a) and DTG (4b) curves of MNP@SC(S)OEt, MNP@PBM, and MNP@PBMS samples. TG curve refers to the temperature-dependent mass change in percent, whereas DTG curve refers to the rate of mass change. The TG curve of the MNP@SC(S)OEt shows total weight loss around 10% in the entire temperature range. This weight loss is related to the decomposition of ethyl xanthate as well as aminosilane shell which is present on MNP surface. After polymerization reactions total weight loss in both samples is higher (51% for MNP@PBM and 30% for MNP@PBMS). TG and DTG curves of MNP@PBM (Figure 4a and 4b) show three stages of weight loss at temperature ranges of 190-320°C, 320–500°C and 700–880°C. The first two ones, with the maxima at 280°C and 390°C are most likely related to the decomposition of carbamohydrazonothioate part, whereas the third one, with the maximum at 800°C, is attributed to the degradation of the polymer chain as well as silica shell. This assumption is based on TG studies of pure monomers which decompose at a broad temperature range between 150/200-650°C (Figure S8 and S14). In the thermograms of the MNP@PBMS sample (Figure 4a and 4b) similar curves characteristics can be observed. However, the rate of mass change is different in this case and the maxima in DTG curve are harder to distinguish comparing to MNP@PBM sample. Two first degradation stages merge into broad peak (150-510°C) with two maxima at 256 and 354°C whereas the third one is slightly shifted to a lower temperature range (650-830°C) with maximum at 710°C. The differences in thermograms of MNP@PBM and MNP@PBMS indicate diverse chemical nature of the polymers surrounding MNP. Comparison of the total weight losses revealed higher polymerization efficiency for BM than for BMS under the applied conditions.

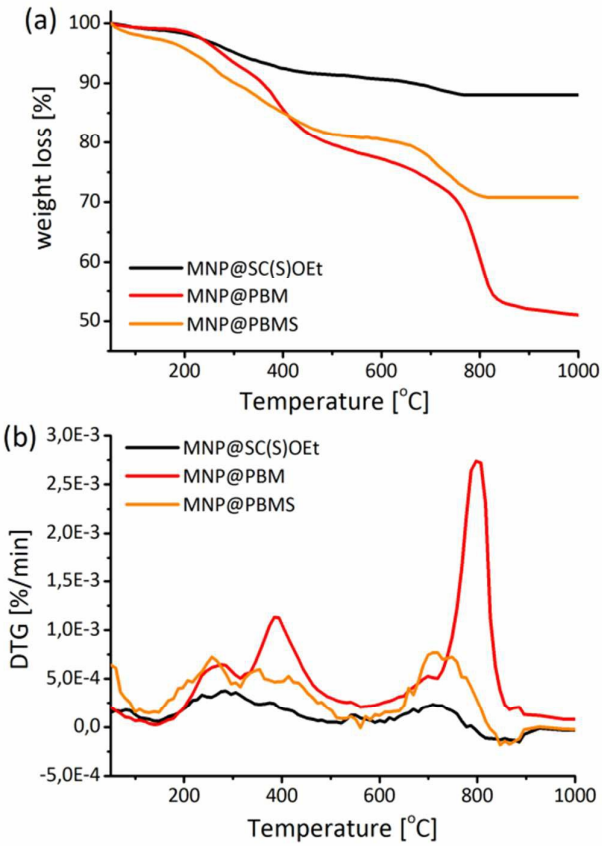

Figure 4. (a) TG and (b) DTG curves of magnetic nanohybrids.

Figure 5 shows TEM and SEM images of MNP@PBM particles. Bare iron oxide nanoparticles are likely to agglomerate and create clusters. Thus, in TEM micrographs, aggregates of magnetic cores (with a relatively narrow size distribution and the average diameter of 10 nm) covered with a shell are observed. The shell surrounding MNP@PBM particles consist of aminosilane and polymer layers and is around 2-3 nm. Similar morphologies were observed in the case

View Article Online
DOI: 10.1039/C6NJ01938B

of MNP@PBMS, however, the thickness of the shell is lower. These results are in a good agreement with the data obtained by TG analysis.

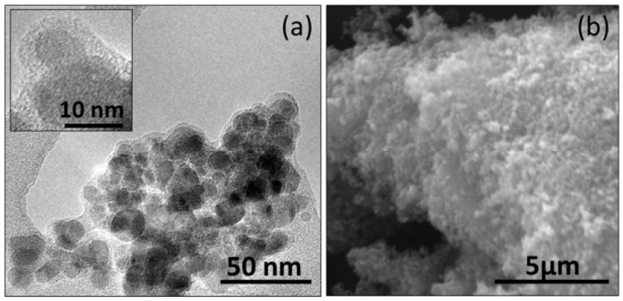

Figure 5. (a) TEM image and (b) SEM image of MNP@PBM particles.

Zeta potential measurements were performed to determine colloidal stability of the obtained nanohybrids. The values of zeta potential for MNP@PBM (11.3 ± 0.6 mV) and MNP@PBMS (37.4 ± 1.1 mV) nanoparticles show that the latter ones are more stable in aqueous dispersion.

Magnetization *versus* field measurements within a range of temperatures revealed that bare nanoparticles exhibit superparamagnetic behaviour at room temperature. In the case of modified MNP increasing the temperature up to the experimentally available maximum of 400 K was necessary to approach the superparamagnetic region and to obtain closing of the hysteretic loops which are still visible at 300 K. Law of approach to saturation (LA) was fitted to the data in high magnetic fields to obtain the values of the saturation magnetisation.[38] Figure 6 shows that the value of the saturation magnetization (M_S) for polymer-coated MNP is reduced in comparison to bare and aminosilane-coated MNP (*e.g.* 62.9 and 48.6 emu g^{-1}, for MNP and MNP@PBM, respectively). These results are consistent with our previous studies which revealed that M_S value mostly depends on the thickness of a shell and barely depends on its composition.[39]

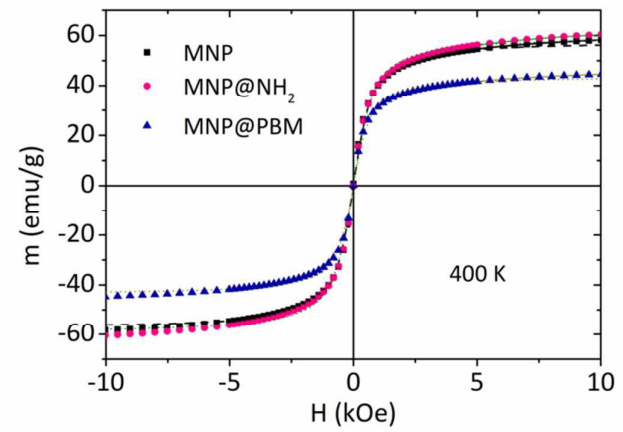

Figure 6. Magnetization as a function of external magnetic field measured for MNP, MNP@NH_2 and MNP@PBM at 400 K. Solid lines represent LA fits to the data.

Complexation of palladium(II) ions. Thiosemicarbazide and their derivatives (*e.g.* thiosemicarbazones) react as complexing ligands with transition metal ions by bonding through the sulphur and hydrazinic nitrogen atom. Obtained in this study monomers are S-substituted, therefore, their chelating abilities are different. However, these monomers (and thus their polymers) possess binding sites such as –NH or –CH=N– able to form metal complexes. To study complexing abilities of the obtained monomers and polymer-coated nanoparticles Pd(II) metal ions were used. Initially, pure monomers were examined in complexation procedures. The solution of metal salt ($2.5 \cdot 10^{-5}$M) was added dropwise to the solution of monomer ($2.5 \cdot 10^{-5}$M). The resulting mixture was tested by UV-Vis spectroscopy to investigate binding action of monomers with metal ions. The spectra of pure monomers show two different transitions with the λ_{max} values around 250 and 300 nm. Slight shifts of the band at 250 nm and vanishing of the band at 300 nm were observed in both cases (Figure S15). Next, in order to investigate their chelating properties, both types of polymer-coated nanoparticles (MNP@PBM and MNP@PBMS) have been tested in the complexation procedures. The suspensions of nanoparticles and solutions of metal ions were shaken under argon atmosphere in room temperature for 24h. The products were magnetically separated and carefully washed few times to rinse all uncomplexed metal salts. UV-Vis analyses performed after this step revealed no significant changes in spectra. It can be related to the fact that nanoparticles themselves (MNP@SC(S)OEt) absorb strongly in the entire tested range.

Thiosemicarbazones have been reported as fluorescent sensors for recognition of transition metal ions.[23,24] Therefore, the fluorescence response of obtained monomers towards metal ions was investigated. Free monomers do not show emission bands whereas their metal complexes show emission maxima around 312/315 nm (Figure S16).

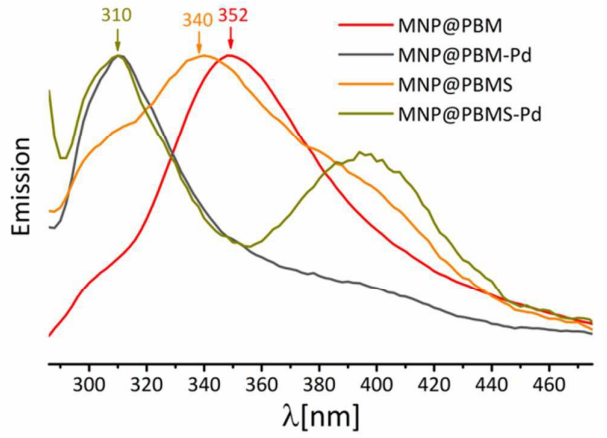

Figure 7. Fluorescence spectra of polymer-modified MNP and their complexes with Pd(II) (normalized to 1).

Figure 7 presents emission spectra of MNP modified with polymers and their complexes with Pd(II). Emission maxima for MNP@PBM and MNP@PBMS samples are observed at 352 and 340 nm, respectively. Introduction of palladium(II) ions caused changes in the emission spectra of nanohybrids, emission maxima in both cases are blue shifted to 310 nm. Additionally, in the spectrum of MNP@PBMS-Pd sample the second maximum at 400 nm appeared.

View Article Online
DOI: 10.1039/C6NJ01938B

Thermogravimetric analyses of MNP@PBM-Pd and MNP@PBMS-Pd samples were performed to estimate the amount of Pd in these samples (Figure 8). In both cases, lower weight loss is observed for complexes than for 'free' polymer-magnetic nanoparticles. It is associated with metal residuals present in these samples. The difference of total weight losses for MNP@PBM and MNP@PBM-Pd is higher than for MNP@PBMS and MNP@PBMS-Pd (20% and 12%) suggesting higher amount of complexed Pd(II) in the former case.

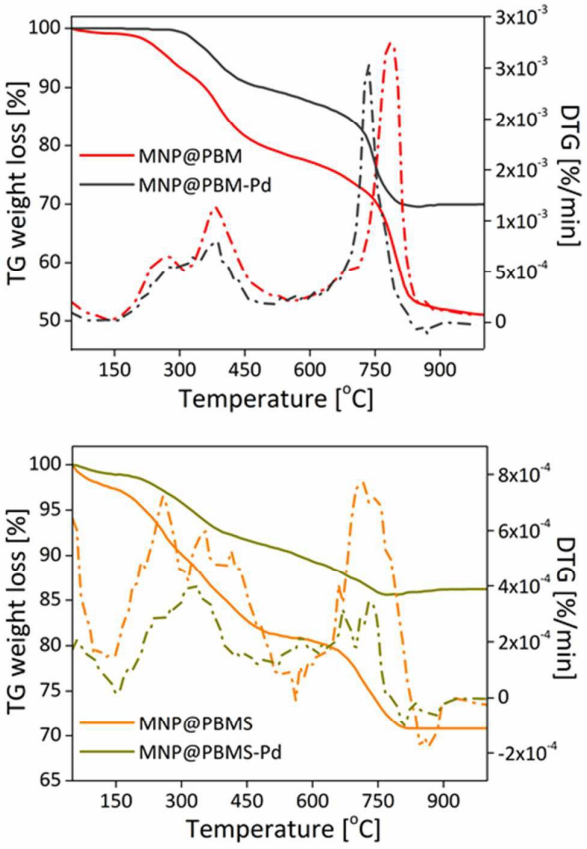

Figure 8. TGA/DTG curves of MNP@PBM, MNP@PBM-Pd, MNP@PBMS, and MNP@PBMS-Pd.

SEM/EDAX analyses were performed to further confirm the presence and estimate the amount of metal ions in MNP@PBM-Pd and MNP@PBMS-Pd samples. According to the results, amount of palladium in MNP@PBM-Pd (19.6±2.1%) sample is roughly twice as high as it is in MNP@PBMS-Pd (9.7±0.5%). It can be related to a different amount of complexing shells (PBM and PBMS) surrounding magnetic cores as well as to different complexing abilities of these layers. Our previous results showed that MNP coated with aminosilane shell do not show complexing activity towards palladium(II).[37]

To study polymerization process of synthesized monomer on MNP@SC(S)OEt nanoparticles a second approach was used. The strategy relied on initial preparation of a ligand-metal complex (BM-Pd) followed by its polymerization on MNP@SC(S)OEt. Polymerization was conducted in the same conditions as in the case of free monomer. Obtained MNP@PBM-Pd(2) particles were examined by FT IR, TGA and SEM/EDX methods and compared to MNP@PBM-Pd sample.

In figure 9a similar set of bands in both spectra as in the MNP@PBM spectrum (Figure 3) can be observed. Pd-Cl stretching frequencies cannot be seen because they normally occur in far infrared region (below 400 cm^{-1}). However, the ratio of intensities of polymer bands (above 1000 cm^{-1}) to magnetic core bands (550 cm^{-1}) is much higher in MNP@PBM-Pd(2) sample. This indicates thicker polymer shell in the case of MNP@PBM-Pd(2) particles and suggests higher efficiency of metal-monomer complex polymerization than free monomer polymerization. TG measurements (Figure 9b) confirmed this data showing higher total weight loss for MNP@PBM-Pd(2) sample (50%) than for MNP@PBM-Pd (30%). SEM/EDX analysis of MNP@PBM-Pd(2) sample revealed 16.59 (±0.53) mass percent of palladium in the sample.

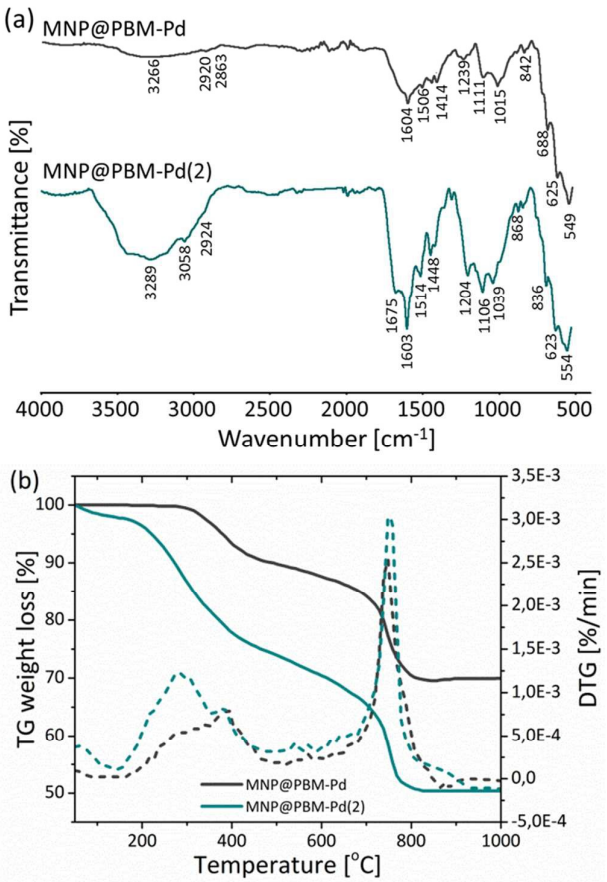

Figure 9. (a) ATR FT IR spectra and (b) TGA/DTG curves of MNP@PBM-Pd and MNP@PBM-Pd(2).

Hemocompatibility of bifunctional monomer and obtained nanoparticles. Thiosemicarbazide-based polymer-magnetic nanohybrids can be used in a range of biomedical applications. However, as nanoparticles may generate various toxic effects in host cells,[40] risk associated with the exposure to these materials has to be evaluated. The hemolytic activity of BM, MNP@SC(S)OEt and MNP@PBM was tested following standard protocols using human red blood cells (RBCs) as the samples.[41] Figure 10 shows results of

View Article Online
DOI: 10.1039/C6NJ01938B

the hemolytic activity measurements. None of tested materials disrupt RBCs membranes at concentrations of 1 to 100 µg/mL (hemolysis rates were lower than 5%).

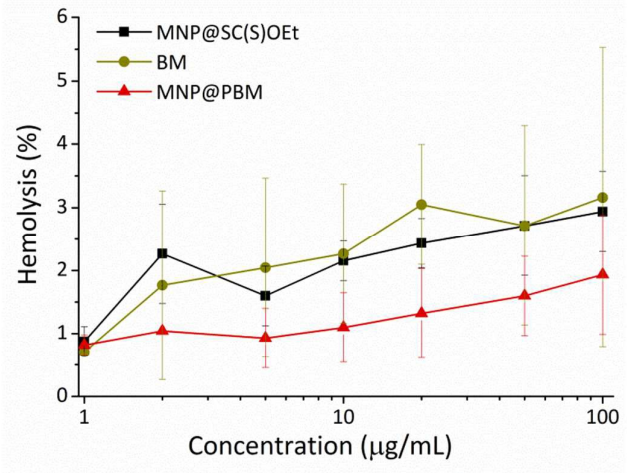

Figure 10. Hemolysis percentages measured at the concentration range of 1-100 µg/mL for BM, MNP@SC(S)OEt, and MNP@PBM incubated with RBCs at 37°C for 1 h.

Conclusions

Herein is presented the formation of new type of chelating-magnetic nanohybrids. These nanohybrids consist of polymers covalently attached to the surface of iron oxide nanocores, therefore, they are stable and resistant to washout. In order to obtain these materials, new polymerizable and complexing monomer based on thiosemicarbazide was synthesized and fully characterized. Next, surface-initiated RAFT/MADIX polymerization reactions of the monomer and its hydrochloric salt (BM and BMS) were performed on xanthate-coated iron oxide nanoparticles (MNP@SC(S)OEt). In both cases formation of polymer coating was documented by FTIR, TEM and TG analyses. To study complexing abilities of MNP@PBM and MNP@PBMS nanohybrids Pd(II) ions were used. The results of SEM/EDX microscopy and TG analysis showed that the content of metal varies depending on the type of shell and it is roughly twice as high in MNP@PBM-Pd as in MNP@PBMS-Pd samples. Additionally, the second approach to polymerization on the surface of dithiocarbonate-coated MNP was applied - bifunctional monomer-metal complex (BM-Pd) was polymerized on MNP@SC(S)OEt. Relatively comparable content of palladium ions was estimated for its MNP@PBM complexes obtained by both approaches. However, the second strategy resulted in higher polymerization efficiency.

The obtained materials due to their combined properties (magnetism and metal affinity) are promising candidates for application in heavy metal ions removal or organic catalysis. It is worth nothing that bactericidal properties of the obtained monomers were successfully tested (in-house data). Additionally, hemolytic activity test results confirmed the possibility of using these nanohybrids in biomedical applications (hemolysis rates were lower than 5%).

Experimental

Materials and methods

Thiosemicarbazide, benzaldehyde, 4-chloromethyl styrene, hydroquinone, and palladium(II) chloride were purchased from Sigma-Aldrich and used as received. Initiator 2,2'-azobis(2-methylpropionitrile) (AIBN) was obtained from MERCK and was recrystallized from chloroform. Triethylamine and all solvents were purchased from Avantor Performance Materials Poland S.A. and were distilled prior use.

The ^{1}H and ^{13}C NMR spectra were recorded on a Bruker Avance spectrometer (400 and 100 MHz, respectively) as solutions in $CDCl_3$, CD_3OD or DMSO. Chemical shifts are expressed in parts per million (ppm, δ) downfield from tetramethylsilane (TMS). FT IR spectra were recorded using Thermo Scientific Nicolet 6700 FT IR spectrophotometer. A thin layer of sample was placed in direct contact with an infrared attenuated total reflection (ATR) diamond crystal. All FT IR spectra were collected in the wavenumber range of 4000 to 500 cm^{-1} by co-adding 32 scans with a resolution of 4 cm^{-1}. Melting points were determined on a Mettler Toledo MP70 system. Elemental analyses were carried out using a VarioMICRO Cube analyzer from Elementar Analysensysteme GmbH. High-resolution mass spectrometry experiments were carried out using a liquid chromatograph (series 1200, Agilent Technologies) coupled to a tandem mass spectrometer (Agilent Technologies 6538 UHD Accurate Mass Q-TOF LC/MS) equipped with a HPLC-chip-cube. Crystals of BM and BMS suitable for single crystal X-ray structural measurement were obtained by slow evaporation of the methanol solution at the room temperature. The X-Ray data were collected on a SuperNova diffractometer (Agilent) with a CCD detector and $Mo_{K\alpha}$ radiation at 100K. The crystal structures were solved with olex2.solve and refine with olex2.refine[42] (BM) and ShelXL (BMS)[43]. All hydrogen atoms were located in electron-density difference maps. The non-hydrogen atoms were refined anisotropically. Transmission electron microscopy photographs were taken on Tecnai G2 X-TWIN microscope. SEM/EDAX measurements were performed on a SEM FEI FP2017/12 Inspect instrument equipped with an Ametek energy dispersive X-ray EDAX Octane Pro system operate at an accelerating voltage of 25 kV. A thin layer of sample was placed on carbon tape and coated with 5 nm layer of gold. Magnetic properties of the nanoparticles were studied using a Quantum Design MPMS 5XL SQUID-type magnetometer. The sample was placed in a standard gelatin capsule and immobilized with Varnish glue for the measurement. All the data were carefully corrected for the diamagnetic contribution of the holder. Thermogravimetric analysis (TGA) was performed on a Mettler Toledo Star TGA/DSC unit. Nitrogen was used as a purge gas (20 $mL \cdot min^{-1}$). Samples between 2 and 10 mg were placed in aluminum pans and heated from 50°C to 800°C (TGA) with a heating rate of 20K/min. Colloidal stability of the obtained materials was studied using the Zetasizer Nano-ZS (Malvern Instruments, Worcestershire, UK) equipped with a 4-mW helium/neon laser (λ = 633 nm) and a thermoelectric temperature controller. Particle suspensions prepared in deionized water (0.05 wt%) were preincubated at 25°C for 5 min before measurement. UV-Vis spectra were taken on Jasco V-670 Spectrophotometer and fluorescence analyses were done on Hitachi F7000 Fluorescence Spectrophotometer (exciation

View Article Online
DOI: 10.1039/C6NJ01938B

wavelength 254 nm). Hemolytic activity was investigated using human red blood cells (RBCs) suspended in phosphate-buffered saline (PBS) (hematocrit ~5%) with a concentration of tested antibacterial agents ranging from 0-100 μg/ml. RBCs were incubated with tested agents for 1 h at 37°C. Relative hemoglobin concentration in supernatants after centrifugation at 2500 rpm for 15 min was monitored by measuring optical absorbance at 540 nm. 100% hemolysis was taken from samples in which 1% Triton X-100 was added to disrupt all cell membranes.

Ethics Statement. Hemolytic activity of tested agents was evaluated in blood samples from adult healthy volunteers under IRB approval: R-I-002/382/2012. This study was approved by the institutional review board (IRB) of The Medical University of Bialystok. All subjects provided informed written consent and collected samples were anonymous.

Synthetic procedures

Synthesis of benzaldehyde thiosemicarbazone (BTSC). Benzaldehyde (6.1 mL, 60 mmol, 1.1 equiv.) was dropped to the solution of thiosemicarbazide (5 g, 55 mmol, 1 equiv.) in anhydrous ethanol (200 mL). The mixture was stirred for 60 h at room temperature under light shielding conditions. Then, the solvent was removed under reduced pressure and obtained crude product was purified by crystallization from ethyl acetate to give yellowish powder (4.1 g, 82%). ^{1}H NMR δ_H(400 MHz, DMSO, Me_4Si): 11.42 (s, 1H, =N-NH), 8.19 (d, J=42 Hz, 2H, NH_2), 8.04 (s, 1H, -CH=N-), 7.81 (m, 2H, H_{Ar}), 7.38 (t, J=3.29 Hz, 3H, H_{Ar}). ^{13}C NMR δ_C(100 MHz, DMSO, Me_4Si): 178.0 (C=S), 142.3(CH), 134.2 (C), 129.8 (CH), 128.7 (2CH), 127.3 (2CH). ATR FTIR (ν_{max}, cm^{-1}): 3399, 3229, 3140 (NH), 3017 (CH_{Ar}), 2975 (=CH), 1599, 1583(NH), 1523, 1468 (SCN), 1446 ($C=C_{Ar}$), 1372 (CH), 1282, 1224, 1098 (CN), 1054 (C=S), 948, 868, 817 (CH_{Ar}), 759, 686, 611, 539 (CS). Elemental analysis. Found: C, 53.88; H, 5.01; N, 23.11; S, 18.03. $C_8H_9N_3S$ requires C, 53.61; H, 5.06; N 23.44; S, 17.89.

Synthesis of vinyl derivative of benzaldehyde thiosemicarbazone (BM). Benzaldehyde thiosemicarbazone (4g, 22 mmol, 1 equiv.) was dissolved in anhydrous ethanol (200 mL), then, 4-chloromethyl styrene (6.3 mL, 45 mmol, 2 eq) was added. The reaction was performed in the presence of Et_3N and hydroquinone at room temperature for 24h under light shielding conditions. The solvent was evaporated under reduced pressure. The product was purified by medium pressure liquid chromatography (MPLC) and crystallization from n-hexane and dichloromethane. Yellowish powder (4-ethenylbenzyl *N*'-[(*E*)-phenylmethylidene]carbamohydrazonothioate) was obtained (5.4 g, 83%). mp = 78.4-79.5°C. ^{1}H NMR δ_H(400 MHz, $CDCl_3$, Me_4Si): 8.43 (s, 1H, HC=N), 7.78 (m, 2H, H-Ar), 7.42 (m, 7H, H-Ar), 6.78 (m, 1H, CH=), 5.79 (d, J=10.87 Hz, 1H, CH_2=), 5.25 (d, J=10.85 Hz, 1H, CH_2=), 4.36 (s, 2H, CH_2-S). ^{13}C NMR δ_C(100 MHz, $CDCl_3$, Me_4Si): 161.1 (C-S), 154.6 (CH), 136.9 (C), 136.7 (C), 136.3 (C), 135.0 (C), 130.0 (CH), 129.2 (CH), 128.5 (CH), 127.7 (CH), 126.4 (CH), 113.9 (CH_2), 34.1 (CH_2). ATR FTIR (ν_{max}, cm^{-1}): 3473, 3362 (NH), 3079, 3057, 3025 (CH_{Ar}), 2936, 2895 (CH), 1966, 1917, 1813 (Ar), 1604 (C=N), 1577, 1523 (NH), 1489, 1446 ($C=C_{Ar}$), 1355, 1305 (CH), 1197, 1172 (CN), 902, 825, 756, 698 (CH_{Ar}), 643 (CS). Elemental analysis. Found: C, 69.03; H, 5.66; N, 13.40; S, 10.84. $C_{17}H_{17}N_3S$ requires C, 69.12; H, 5.8; N, 14.22; S, 10.85. LC MS/MS (ESI) m/z found 296.1220 $[C_{17}H_{17}N_3S+H]^+$; calculated 296.1216.

Synthesis of vinyl derivative of benzaldehyde thiosemicarbazone salt (BMS). HCl was dropped to BM solution in $CHCl_3$. Precipitation of yellow powder was observed. The product (*1E*,*2E*)-1-{amino[(4-ethenylbenzyl)sulfanyl]methylidene}-2-benzylidenehydrazinium chloride was recrystallized from methanol. mp = 176.1-177.9°C. ^{1}H NMR δ_H(400 MHz, CD_3OD, Me_4Si): 8.28 (s, 1H, HC=N), 7.78 (m, 2H, H-Ar), 7.38 (m, 7H, H_{Ar}), 6.78 (m, 1H, CH=), 5.77 (d, J=17.65 Hz, 1H, CH_2=), 5.21 (d, J=10.88 Hz, 1H, CH_2=), 4.29 (s, 2H, CH_2-S). ^{13}C NMR δ_C(100 MHz, CD_3OD, Me_4Si): 162.7 (C-S), 152.2 (CH), 136.6 (C), 136.1 (C), 133.4 (CH), 131.0 (CH), 129.3 (CH), 128.7 (CH), 126.4 (CH), 114.6 (CH_2), 34.1 (CH_2). ATR FTIR (ν_{max}, cm^{-1}): 3362 (NH), 3038 (CH_{Ar}), 2971 (CH), 1645 (C=N), 1581, 1511 (NH), 1447, 1408 ($C=C_{Ar}$), 1135 (CN), 1051, 758, 688 (CH_{Ar}), 617(CS). Elemental analysis. Found: C, 59.48; H, 5.57; N, 11.50; S, 9.06. $C_{18}H_{22}N_3SClO$ requires C, 59.41; H, 6.09; N, 11.55; S, 8.81.

General procedure for free radical polymerization. Monomer (BM or BMS) and solvent (THF or ethanol) were placed in a flask equipped with a magnetic stirrer and were degassed for 15 min by bubbling argon. Then, AIBN was added and solution was heated at 60°C/80°C for 24h under argon gas protection. During reactions precipitation of yellow poorly soluble fractions was observed. PBM ^{1}H NMR δ_H(400 MHz, $CDCl_3$, Me_4Si): 8.07-8.01 (HC=N), 7.60-7.00 (H_{Ar}), 4.39-4.11 (CH_2-S), 1.81-1.08 (CH-CH_2). PBMS ^{1}H NMR δ_H(400 MHz, CD_3OD, Me_4Si): 8.04-8.01 (HC=N), 7.50-6.50 (H_{Ar}), 4.36-4.34 (CH_2-S), 1.81-1.26 (CH-CH_2).

General procedure for RAFT/MADIX polymerization with *O*-ethyl-*S*-(1-methoxycarbonyl)ethyldithio-carbonate. *O*-ethyl-*S*-(1methoxy carbonyl)ethyldithiocarbonate, monomer (BM or BMS) and solvent (THF or ethanol) were placed in a flask equipped with a magnetic stirrer and were degassed for 15 min by bubbling argon. Then, AIBN was added and solution was heated at 60°C/80°C for 24h under argon gas protection. During reactions precipitation of yellowish poorly soluble fractions was observed. PBM-SC(S)OEt ^{1}H NMR δ_H(400 MHz, DMSO, Me_4Si): 8.10-7.97 (HC=N), 7.50-7.30 (H_{Ar}), 4.41-4.37 (CH_2-O), 3.77-3.76 (CH-COO), 3.17-3.14 (CH_2-S), 1.55-1.00 (CH_2, CH). PBMS-SC(S)OEt ^{1}H NMR δ_H(400 MHz, CD_3OD, Me_4Si): 7.90-7.80 (HC=N), 7.60-7.30 (H_{Ar}), 4.50-4.43 (CH_2-O), 3.70-3.60 (CH-COO), 3.20-3.10 (CH_2-S), 1.55-1.10 (CH_2,CH).

General procedure for polymerization on MNP@SC(S)OEt. A typical polymerization procedure was as follows: a mixture of MNP@SC(S)OEt, monomer (BM or BMS), solvent and AIBN was sonicated under argon gas protection until a homogeneous suspension was formed. Next, it was transferred into an oil bath and stirred at the constant temperature at 60°C/80°C. After 48h, the polymerization was stopped by diluting the mixture in solvent and magnetic decantation. The cycle of redispersion and magnetic separation was repeated several times to rinse free polymer chains and obtain "pure" polymer-grafted nanoparticles. MNP@PBM ATR FTIR (ν_{max}, cm^{-1}): 3300 (NH), 3059 (CH_{Ar}), 2927 (CH), 1666 (NH), 1416 (CH) 1112, 1015 (SiO), 557 (FeO). MNP@PBMS ATR FTIR (ν_{max}, cm^{-1}): 3332 (NH), 2921, 2850 (CH), 1646 (NH), 1444 (CH), 1113, 1042 (SiO), 565 (FeO).

Acknowledgements

View Article Online
DOI: 10.1039/C6NJ01938B

This work was financially supported by the National Science Centre, Poland, grants no. NCN/2011/03/B/ST5/02691 (AZW) and 2014/13/N/ST5/01563 (KHM). The equipment in The Center of Synthesis and Analysis BioNanoTechno of University of Bialystok was funded by EU, project no: POPW.01.03.00–20–034/09–00 and POPW.01.03.00-004/11. The authors gratefully acknowledge use of the mass spectrometry services and facilities of the Center for Interdisciplinary Research of The John Paul II Catholic University of Lublin, funded by POPW.01.03.00-06-003/09-00. The authors are grateful to Dr Katarzyna Niemirowicz for hemolysis tests.

References

1 D. Pandiarajan, R. Ramesh, Y. Liu and R. Suresh, *Inorg. Chem. Commun.*, 2013, **33**, 33–37.
2 L. Wang, M. Cole, J. Li, Y. Zheng, Y. P. Chen, K. P. Miller, A. W. Decho and B. C. Benicewicz, *Polym Chem*, 2015, **6**, 248–255.
3 A. A. Atia, A. M. Donia and A. M. Yousif, *Sep. Purif. Technol.*, 2008, **61**, 348–357.
4 M. Beija, J.-D. Marty and M. Destarac, *Prog. Polym. Sci.*, 2011, **36**, 845–886.
5 S. Datta, D. K. Seth, S. Gangopadhyay, P. Karmakar and S. Bhattacharya, *Inorganica Chim. Acta*, 2012, **392**, 118–130.
6 S. Dutta, F. Basuli, A. Castineiras, S.-M. Peng, G.-H. Lee and S. Bhattacharya, *Eur. J. Inorg. Chem.*, 2008, **2008**, 4538–4546.
7 D. Kovala-Demertzi, P. N. Yadav, M. A. Demertzis, J. P. Jasiski, F. J. Andreadaki and I. D. Kostas, *Tetrahedron Lett.*, 2004, **45**, 2923–2926.
8 Y. Kurt and N. G. Deniz, *J. Coord. Chem.*, 2015, **68**, 4070–4081.
9 P. Paul, R. J. Butcher and S. Bhattacharya, *Inorganica Chim. Acta*, 2015, **425**, 67–75.
10 R. N. Prabhu and R. Ramesh, *Tetrahedron Lett.*, 2012, **53**, 5961–5965.
11 N. Raja and R. Ramesh, *Spectrochim. Acta. A. Mol. Biomol. Spectrosc.*, 2010, **75**, 713–718.
12 J. S. Casas, M. S. García-Tasende and J. Sordo, *Coord. Chem. Rev.*, 2000, **209**, 197–261.
13 T. S. Lobana, R. Sharma, G. Bawa and S. Khanna, *Coord. Chem. Rev.*, 2009, **253**, 977–1055.
14 A. Sankaraperumal, J. Karthikeyan, A. N. Shetty and R. Lakshmisundaram, *Polyhedron*, 2013, **50**, 264–269.
15 S., Neelam Bharti, F. Naqvi and A. Azam, *Bioorg. Med. Chem. Lett.*, 2003, **13**, 689–692.
16 C. Soykan and ?brahim Erol, *J. Polym. Sci. Part Polym. Chem.*, 2003, **41**, 1942–1951.
17 P. Genova, T. Varadinova, A. I. Matesanz, D. Marinova and P. Souza, *Toxicol. Appl. Pharmacol.*, 2004, **197**, 107–112.
18 J. R. Dilworth and R. Hueting, *Inorganica Chim. Acta*, 2012, **389**, 3–15.
19 P. J. Jansson, D. S. Kalinowski, D. J. R. Lane, Z. Kovacevic, N. A. Seebacher, L. Fouani, S. Sahni, A. M. Merlot and D. R. Richardson, *Pharmacol. Res.*, 2015, **100**, 255–260.
20 F. Vandresen, H. Falzirolli, S. A. Almeida Batista, A. P. B. da Silva-Giardini, D. N. de Oliveira, R. R. Catharino, A. L. T. G. Ruiz, J. E. de Carvalho, M. A. Foglio and C. C. da Silva, *Eur. J. Med. Chem.*, 2014, **79**, 110–116.
21 B. S. Garg and V. K. Jain, *Microchem. J.*, 1988, **38**, 144–169.
22 S. L. Ashok Kumar, M. Saravana Kumar, P. B. Sreeja and A. Sreekanth, *Spectrochim. Acta. A. Mol. Biomol. Spectrosc.*, 2013, **113**, 123–129.
23 D. Udhayakumari, S. Suganya and S. Velmathi, *J. Lumin.*, 2013, **141**, 48–52.
24 S. Suganya, D. Udhayakumari and S. Velmathi, *Anal. Methods*, 2013, **5**, 4179–4183.
25 M. Destarac, C. Brochon, J.-M. Catala, A. Wilczewska and S. Z. Zard, *Macromol. Chem. Phys.*, 2002, **203**, 2281–2289.
26 D. Taton, A.-Z. Wilczewska and M. Destarac, *Macromol. Rapid Commun.*, 2001, **22**, 1497–1503.
27 S. Perrier and P. Takolpuckdee, *J. Polym. Sci. Part Polym. Chem.*, 2005, **43**, 5347–5393.
28 M. Destarac, *Macromol. React. Eng.*, 2010, **4**, 165–179.
29 Y. Zhao and S. Perrier, in *Controlled Radical Polymerization at and from Solid Surfaces*, ed. P. Vana, Springer International Publishing, Cham, 2015, vol. 270, pp. 77–106.
30 Y. He, Y. Huang, Y. Jin, X. Liu, G. Liu and R. Zhao, *ACS Appl. Mater. Interfaces*, 2014, **6**, 9634–9642.
31 G. Huang, Z. Sun, H. Qin, L. Zhao, Z. Xiong, X. Peng, J. Ou and H. Zou, *The Analyst*, 2014, **139**, 2199–2206.
32 A. Z. Wilczewska and K. H. Markiewicz, *Macromol. Chem. Phys.*, 2014, **215**, 190–197.
33 I. Misztalewska, A. Z. Wilczewska, O. Wojtasik, K. H. Markiewicz, P. Kuchlewski and A. M. Majcher, *RSC Adv*, 2015, **5**, 100281–100289.
34 C. Li, L.-Z. Meng, X.-J. Lu, Z.-Q. Wu, L.-F. Zhang and Y.-B. He, *Macromol. Chem. Phys.*, 2005, **206**, 1870–1877.
35 X. Lu, S. Gong, L. Meng, C. Li, F. Liang, Z. Wu and L. Zhang, *Eur. Polym. J.*, 2007, **43**, 2891–2900.
36 O. V. Dolomanov, L. J. Bourhis, R. J. Gildea, J. A. K. Howard and H. Puschmann, *J. Appl. Crystallogr.*, 2009, **42**, 339–341.
37 A. Z. Wilczewska and I. Misztalewska, *Organometallics*, 2014, **33**, 5203–5208.
38 V. A. Ignatchenko, R. S. Iskhakov and G. V. Popov, *Sov. Phys. – JETP*, 1982, **55**, 878–886.
39 I. Misztalewska, A. Z. Wilczewska, O. Wojtasik, K. H. Markiewicz, P. Kuchlewski and A. M. Majcher, *RSC Adv*, 2015, **5**, 100281–100289.
40 Y.-X. J. Wang, Zhu, Leung, Lee, Zhao, Wang, Lai, Wan, C. H. K. Cheng and Ahuja, *Int. J. Nanomedicine*, 2012, 953–964.
41 K. Niemirowicz, I. Swiecicka, A. Z. Wilczewska, K. H. Markiewicz, U. Surel, A. Kułakowska, Z. Namiot, B. Szynaka, R. Bucki and H. Car, *Colloids Surf. B Biointerfaces*, 2015, **131**, 29–38.
42 L. J. Bourhis, O. V. Dolomanov, R. J. Gildea, J. A. K. Howard and H. Puschmann, *Acta Crystallogr. Sect. Found. Adv.*, 2015, **71**, 59–75.
43 G. M. Sheldrick, *Acta Crystallogr. A*, 2008, **64**, 112–122.

View Article Online
DOI: 10.1039/C6NJ01938B

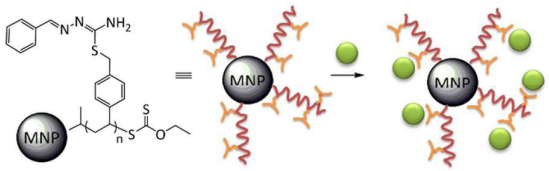

Complexing and easily separable polymer-magnetic nanohybrids based on iron oxide nanoparticles and original carbamohydrazonothioate derivatives.